RSC Advances

PAPER

View Article Online
View Journal | View Issue

Cite this: *RSC Adv.*, 2020, **10**, 12119

Development of a turn-on graphene quantum dot-based fluorescent probe for sensing of pyrene in water†

Nsibande S. A. and Forbes P. B. C.*

Polycyclic aromatic hydrocarbons (PAHs) are potentially harmful pollutants that are emitted into the environment from a range of sources largely due to incomplete combustion. The potential toxicity and carcinogenic effects of these compounds warrants the development of rapid and cost-effective methods for their detection. This work reports on the synthesis and use of graphene quantum dots (GQDs) as rapid fluorescence sensors for detecting PAHs in water. The GQDs were prepared from two sources, *i.e.* graphene oxide (GO) and citric acid (CA) – denoted GO-GQDs and CA-GQDs, respectively. Structural and optical properties of the GQDs were studied using TEM, Raman, and fluorescence and UV-vis spectroscopy. The GQDs were then applied for detection of pyrene in environmental water samples based on a "turn-off-on" mechanism where ferric ions were used for turn-off and pyrene for turn-on of fluorescence emission. The fluorescence intensity of both GQDs was switched on linearly within the 2–10 $\times$ 10^{-6} mol L^{-1} range and the limits of detection were found to be 0.325 $\times$ 10^{-6} mol L^{-1} and 0.242 $\times$ 10^{-6} mol L^{-1} for GO-GQDs and CA-GQDs, respectively. Finally, the potential application of the sensor for environmental water samples was investigated using lake water and satisfactory recoveries (97–107%) were obtained. The promising results from this work demonstrate the feasibility of pursuing cheaper and greener environmental monitoring techniques.

Received 4th December 2019
Accepted 19th March 2020

DOI: 10.1039/c9ra10153e

rsc.li/rsc-advances

1. Introduction

Polycyclic aromatic hydrocarbons (PAHs) are a class of organic compounds with fused benzene rings which are of environmental concern. These compounds can be introduced into environmental compartments (water, soil, sediments and air) through various pathways including industrial activities, biomass burning, and vehicular emissions, amongst others. A number of comprehensive studies have documented the occurrence of PAHs in a variety of matrices, including water.[1–7]

The environmental monitoring of these compounds continues to be of importance due to their potential negative health effects, as some PAHs have been reported to be either carcinogenic or potentially carcinogenic.[8–10] The toxicity of a number of PAH compounds can further be enhanced upon their metabolism and photooxidation into derivative compounds.[4,11] Moreover, in aquatic systems, where PAHs normally occur as mixtures, they can have increased toxicity compared to individual PAHs due to synergistic effects.[12]

The low solubility of PAHs in water means that they typically occur at low concentrations in environmental samples, thus sensitive analytical techniques are required for monitoring of these compounds. Traditionally, chromatographic techniques are used as 'gold standards' for monitoring and quantification of PAHs. However, these techniques can be expensive especially where routine monitoring is required. As an alternative to chromatographic techniques, researchers have been investigating the use of various nanomaterials as sensors and/or platforms for sensitive detection of PAHs, as recently reviewed.[13]

Graphene materials have been widely explored in developing sensors for PAHs. We previously demonstrated the potential use of semiconductor quantum dots coupled to graphene oxide to form conjugate platforms for fluorescence detection of PAHs,[14,15] for example. The success of such sensors was attributed to the excellent fluorescence properties QDs (including high quantum yields and photostability) and the ability to modify their surfaces with desired functionalities, such as the formation of a nanocomposite with graphene oxide to enhance interaction with PAHs. However, the major drawback of these sensors is the use of heavy metals like cadmium which have the potential to leach from the sensor material and raise environmental and health concerns.

In recent years, graphene quantum dots (GQDs) have emerged as a possible alternative to semiconductor QDs. GQDs can be regarded as extremely small, zero-dimensional pieces of graphene which have quantum confinement and edge effect properties similar to carbon dots.[16] The fluorescence properties

Chemistry Department, Faculty of Natural and Agricultural Sciences, University of Pretoria, South Africa. E-mail: patricia.forbes@up.ac.za

† Electronic supplementary information (ESI) available. See DOI: 10.1039/c9ra10153e

of GQDs arise from the radiative recombination of electron–hole (e–h) pairs in sp^2 aromatic carbon sites. This is because graphene has infinitely large Bohr diameters (distance between electron and hole) and therefore its fragments, *i.e.* GQDs, of any size exhibit quantum confinement effects.[17]

These GQDs have certain advantageous properties over semiconductor QDs, including higher photostability, biocompatibility, large surface area, better surface grafting using π–π conjugation and surface groups, and they have lower toxicity[18–20] which has allowed for their use in biological applications.[21] Thus GQDs have recently found extensive application in the design of sensing probes.[18,22–24] Moreover, GQDs can be easily prepared using various synthesis routes, which can be categorized into two main categories; namely the "top-down" approach or the "bottom-up" approach. The top-down approach involves the breaking of bulk macroscopic carbon materials (like graphite, carbon fibers, graphene oxide, metal–organic frameworks, *etc.*) usually through harsh oxidation treatments or lithography techniques. The bottom-up approach involves growing GQDs from small molecular precursors (like citric acid, glucose, PAHs, *etc.*) through controlled reactions to obtain desired GQDs nanosizes.[18,23,25] These two approaches have been widely used by researchers and they each have pros and cons depending on the intended application and availability of raw materials.

To this end, the analytical application of GQDs has mostly been towards metal ions sensing[26] with few studies reporting their use for organic pollutant detection like pentachlorophenol,[27] trinitrotoluene[28] and the pesticide tributyltin.[29]

In the this work therefore, we report on the use of GQDs with associated ferric ions for fluorescence detection of PAHs in environmental water samples. Two GQD synthetic approaches were explored for comparison, where those made from citric acid are denoted CA-GQDs, and those prepared from graphene oxide are denoted GO-GQDs. The GQDs were then applied to the detection of pyrene, a four-ring PAH, in environmental water samples for the first time. A fluorescence "turn-off-on" detection strategy was used where ferric ions were used to turn off the fluorescence of the GQDs and subsequent contact with pyrene switched the fluorescence back on.

2. Materials and methods

2.1 Equipment and reagents

Fluorescence emission spectra were recorded on a Horiba Jobin Yvon Fluoromax-4 Spectrofluorometer (Horiba Instruments Inc., Edison, NJ, USA). UV-vis absorption spectra were recorded on a Cary Eclipse spectrophotometer (Varian Pty Ltd, Australia). FTIR spectra were measured using a Bruker Alpha-T spectrometer (Bruker Optik GmbH, Ettlingen, Germany). Transmission electron microscopy (TEM) images were taken using a JEOL JEM 2100F (JOEL Ltd, Tokyo, Japan) operated at 200 kV. The ImageJ software was used to analyse particle size distribution. Raman spectra were recorded with a Horiba T64000 spectrometer (Horiba Jobin Yvon, France) using a 514 nm laser source operated at 0.020 W. SnakeSkin™ dialysis tubing (3.5 kDa MCOW) was purchased from Thermo Fisher Scientific. Polytetrafluoroethylene micro-filters (0.22 μm and 0.45 μm) were purchased from Stargate Scientific.

Citric acid (CA), sodium hydroxide (NaOH), hydrochloric acid (HCl), iron III chloride ($FeCl_3$), potassium permanganate ($KMnO_4$), sodium nitrate ($NaNO_3$), sulphuric acid (H_2SO_4) and hydrogen peroxide (H_2O_2) were all purchased from Sigma-Aldrich. Deionized (DI) water for all experiments was obtained from a Millipore Direct-Q® 3 UV system (Molsheim, France).

The fluorescence quantum yield for all GQDs was calculated by comparing the fluorescence integrated intensities of the GQDs in water to that of a reference standard, namely pyrene, in ethanol.[30]

$$\Phi_x = \Phi_{std}\left(\frac{m_x}{m_{std}}\right)\left(\frac{{n_x}^2}{{n_{std}}^2}\right)$$

where Φ_x is the quantum yield of GQDs, Φ_{std} is the quantum yield of the reference standard, (0.65 in this case), m_x and m_{std} are gradients for the plot of integrated fluorescence intensities *vs.* absorbances for GQDs and standard, respectively, and n refers to the refractive indices of the solvents.

2.2 Bottom-up synthesis of CA-GQDs

GQDs were prepared from citric acid (CA) *via* direct pyrolysis[31] as illustrated in Fig. 1. Briefly, about 2 g of CA was placed in a beaker and heated to ~200 °C on a hot plate. After about 5 min the CA turned into a transparent solution and after a further 15 min of heating it turned pale yellow, suggesting formation of GQDs. The reaction was then stopped followed by slow addition of NaOH (0.25 mol L^{-1}) while stirring vigorously at 300 rpm with a magnetic stirrer. The pH was then adjusted to pH 7 using NaOH and HCl as required, and the resulting pale-yellow solution was purified through dialysis tubing for 2 days to remove unreacted citric acid and excess Na^+ and Cl^- ions. The obtained solution was stored in the refrigerator for further use and analysis.

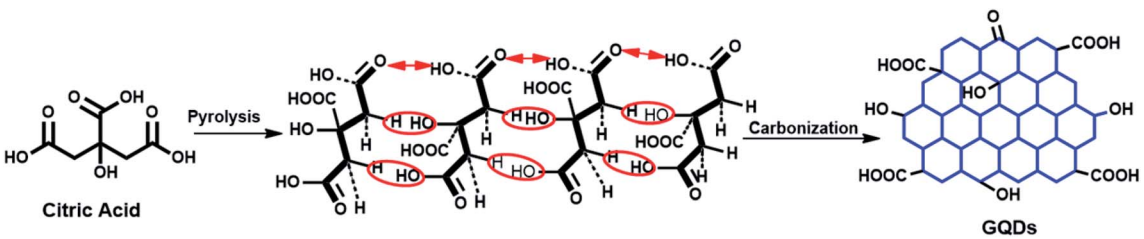

Fig. 1 Schematic illustration of the synthesis of fluorescent GQDs from citric acid through pyrolysis and carbonization.

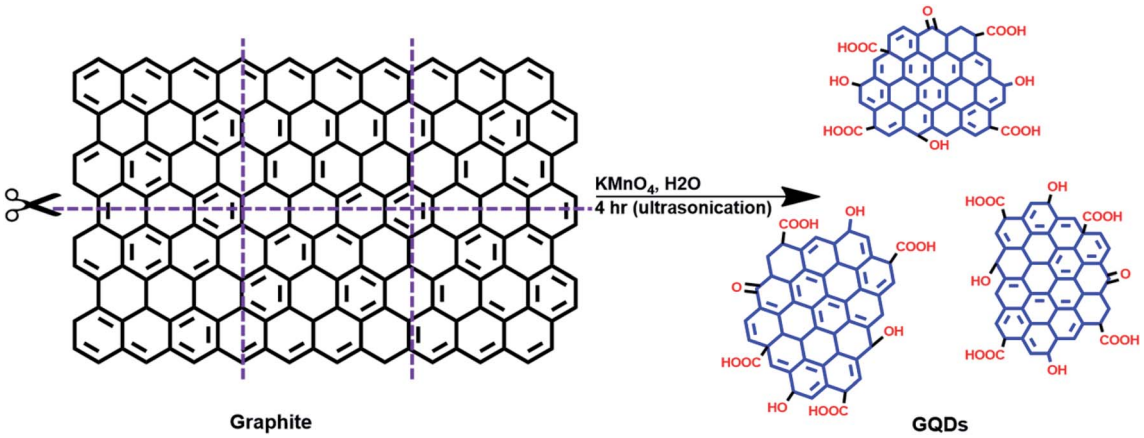

Fig. 2 Schematic illustration of the top-down preparation of GQDs through oxidation of graphene oxide.

2.3 Top-down synthesis of GO-GQDs

Graphene oxide (GO) was first prepared from graphite powder using a modified Hummers' method.[32] In a 250 mL round-bottom flask which was placed in an ice bath, 60 mL of H_2SO_4 was added followed by 2.5 g of graphite powder and 1.25 g of $NaNO_3$. This mixture was stirred vigorously to allow for dispersion of the graphite. Then 7.5 g of $KMnO_4$ was added and after stirring for a few hours the ice bath was removed and the mixture was stirred at room temperature overnight resulting in formation of a brownish mixture. 75 mL of DI water was gradually added to this mixture, which was then allowed to stir overnight. The following day, 25 mL of 30% H_2O_2 was added

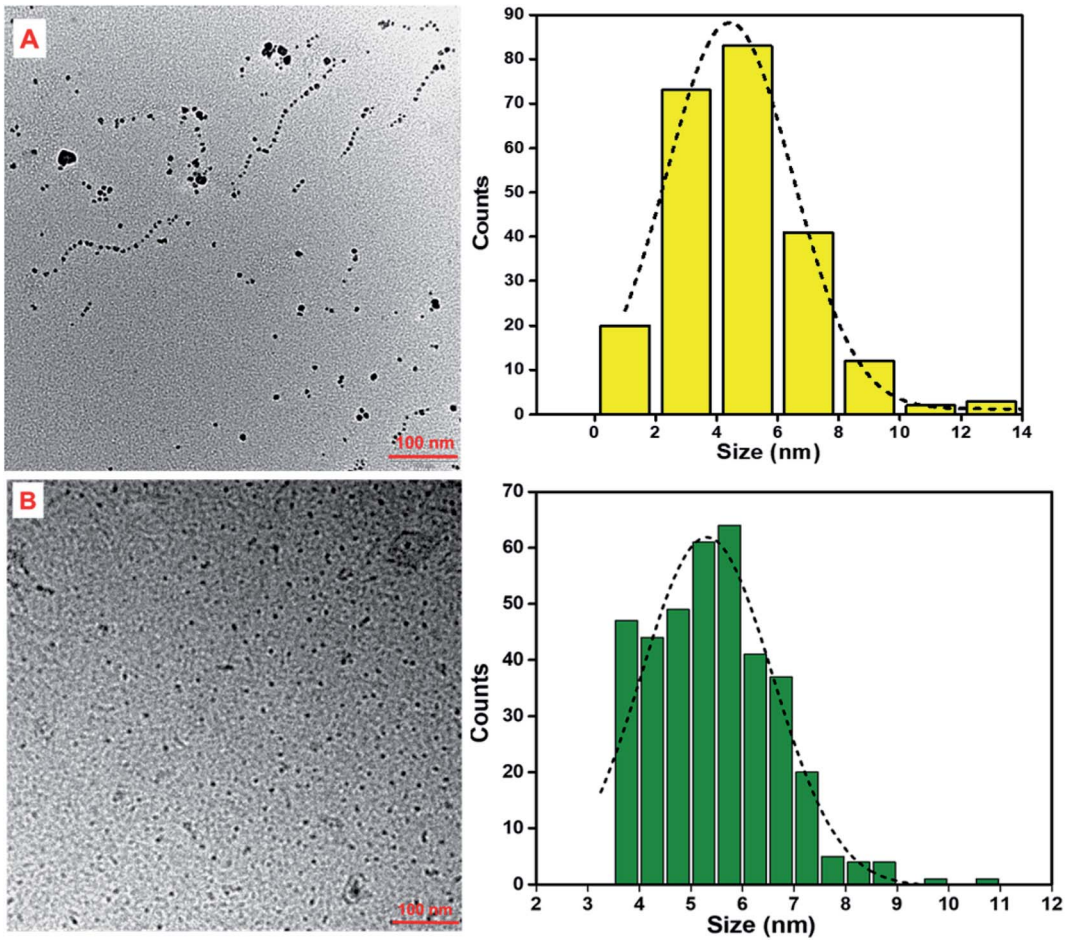

Fig. 3 (a) TEM images of (A) CA-GQDs and (B) GO-GQDs with corresponding particle size distributions (right). The average size for CA-GQDs was 4.8 ± 0.1 nm and 5.5 ± 0.3 nm for GO-GQDs.

and the mixture was then centrifuged and washed first with 5% HCl then with DI water to remove excess unreacted reactant metal ions. The obtained GO powder was dried in an oven at 65 °C and subsequently used to prepare GQDs.

The synthesis of GQDs from GO was carried out using previously reported methods with some modifications[33] and is schematically shown in Fig. 2. Briefly, in a round-bottom flask, 0.050 g of graphene oxide (GO) was mixed with 0.050 g $KMnO_4$ followed by addition of 100 mL of water to form a homogenous mixture. This mixture was then sonicated for 4 h to ensure complete oxidation. Then the mixture was centrifuged at 500 rpm for 10 min to remove large unreacted GO. The supernatant was then filtered first with a 0.45 μm filter PTFE then with a 0.22 μm filter to obtain the GQD solution (Fig. S1†). The solution was further purified by dialysis against deionized water using a 3.5 kDa membrane to remove excess salts and was stored in the refrigerator (at ~4 °C) for further use and characterization. The GQDs prepared through this method are denoted by GO-GQDs.

2.4 Fluorescence detection of pyrene

GQDs have been widely used as sensors for selective detection of Fe^{3+} ions.[34–36] The ability of Fe^{3+} to induce fluorescence quenching has been attributed to coordination of the ferric ions with surface hydroxyl groups of GQDs to form aggregates like iron hydroxides.[37] In this work, the quenched GQDs–Fe aggregates were then used for fluorescence turn-on detection of pyrene. A fixed amount of Fe^{3+} solution (50 μL of 30 μg L^{-1}) was introduced to 400 μL of GQD solution (~0.5 mg mL^{-1}) and 1 min time interval was allowed for interaction. Thereafter 200 μL of different pyrene concentrations (2–10 × 10^{-6} mol L^{-1}) were individually added and an incubation time of 5 min was allowed before fluorescence measurements were recorded. For

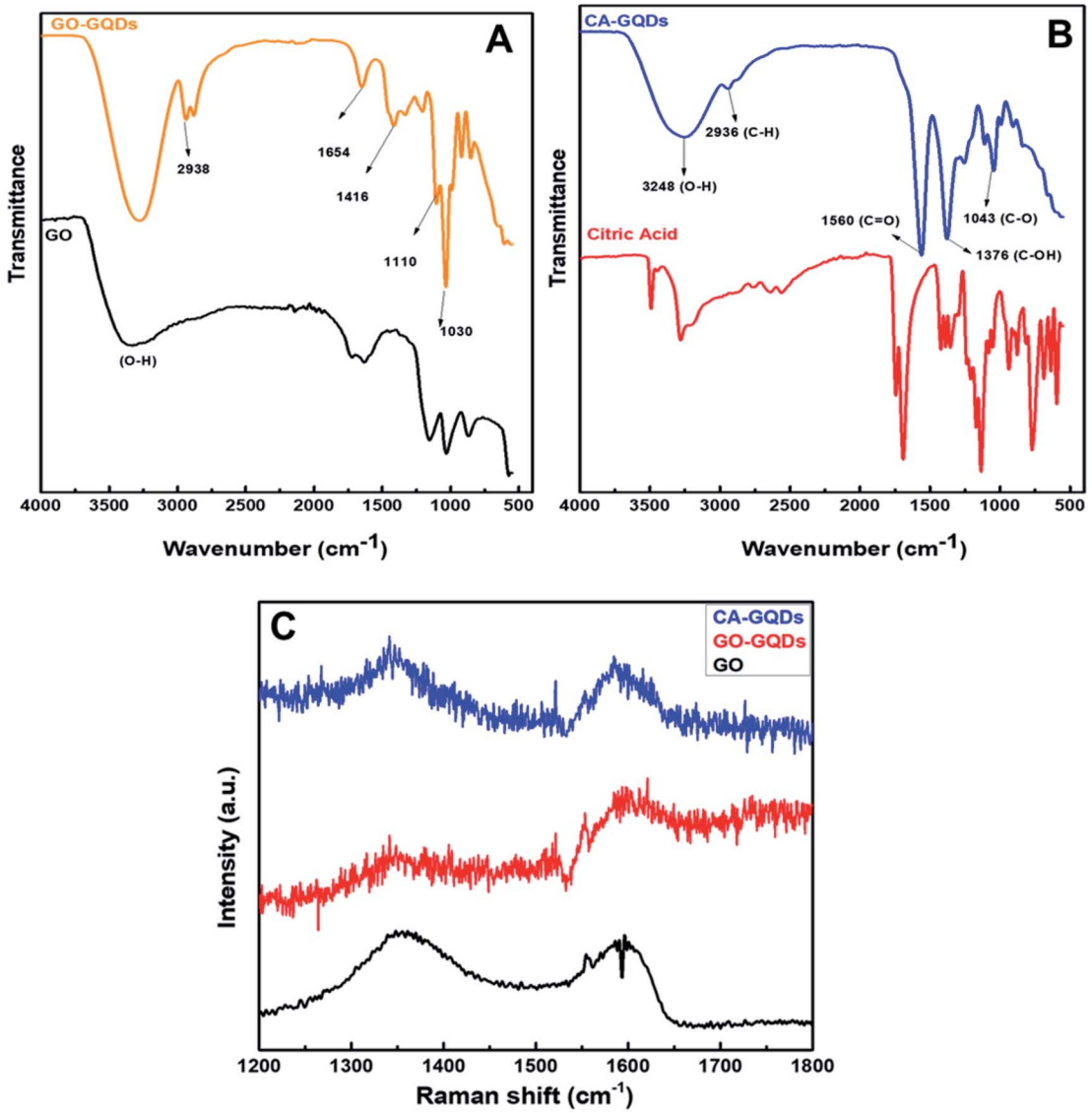

Fig. 4 FTIR spectra of both GO-GQDs (A) and CA-GQDs (B) and their respective precursors. (C) Raman spectra of graphene oxide (GO), CA-GQDs and GO-GQDs.

all PL measurements, the excitation wavelength was 320 nm and both the excitation and emission slit widths were set at 5 nm. The performance of the sensor was tested for real environmental water samples using water from a small lake within the University of Pretoria's Sports Campus. The samples were filtered through a 0.45 μm filter to remove any entrained sediments or suspended material, and aliquots were then spiked at three different concentrations (3, 6 and 10 × 10^{-6} mol L^{-1}) within the calibration curve and were then analyzed in the same manner as standard solutions.

3. Results and discussion

3.1 TEM analysis

Transmission electron microscopy (TEM) analysis was conducted to investigate the particle shape, size and distribution. As can be seen in Fig. 3, both types of GQDs have various polygon-like shapes which indicate formation of thin graphene-like structures during synthesis. The particles were also well dispersed in water and this can be attributed to the presence of –COOH groups on the edges thereof. The average particle size was found to be 4.8 ± 0.1 nm and 5.5 ± 0.3 nm for CA-GQDs and GO-GQDs, respectively.

3.2 FTIR analysis

FTIR analysis was carried out to characterize the type of functional groups that were present in the QDs as shown in Fig. 4A and B, where the characteristic vibrational modes of citric acid are also shown for comparison. The broad band around 3248 cm^{-1} can be attributed to hydroxyl groups, and the 2936 cm^{-1} bands are due to both sp^2 and sp^3 C–H stretching modes. The bands at 1560, 1376 and 3248 cm^{-1} indicate the presence of C=O and C–O groups. The observed bands correspond to those reported in previous studies on GQDs prepared from citric acid.[38] It should also be noted that there was no detected C–O–C stretching vibration which confirms that the carbonization process was terminated before the formation of graphene oxide.

3.3 Raman analysis

It must be noted that the fluorescent emission from the GQDs can mask the Raman signal resulting in a poor signal-to-noise ratio. In this case, a 514 nm laser was used, and to minimize the effect of fluorescence on the Raman peaks the laser power was reduced. The Raman spectra of the GQDs (Fig. 4C) show the characteristic D and G bands at 1349 cm^{-1} and 1590 cm^{-1}, respectively. The D-band can be attributed to disordered sp^3 carbons and the G-band is due to in-plane stretching vibrations of crystalline graphite carbons. The ratio of the intensities of the D and G bands (I_D/I_G) can be used to infer information about the degree of crystallinity and abundance of core carbon and surface carbon atoms. For CA-GQDs and GO-GQDs the I_D/I_G ratio was 1.02 and 0.95, respectively. This high ratio confirms the presence of defects in the structure of the GQDs and a partially disordered crystal structure from the small sp^2 cluster sizes.

3.4 Absorption and fluorescence properties

The absorption and fluorescence emission spectra of both GO-GQDs and CA-GQDs are presented in Fig. 5. As can be seen, both sets of GQDs show the typical broad absorption in the UV region with a tail that extends to the visible range. The GO-GQDs show two shoulder peaks at 230 and 300 nm. The CA-GQDs on the other hand show a distinct peak around 250 nm followed by a broad shoulder at 350 nm. In both cases, the absorption peaks at lower wavelengths can be attributed to π–π electronic transitions of the aromatic C–C bonds in their structure. The absorption shoulder peaks at higher wavelengths can be attributed the functional groups on their edges, specifically π*–n transitions of the C=O bonds.[17,39]

The GQDs showed strong fluorescence emission peaks at 500 nm and 460 nm for GO-GQDs and CA-GQDs, respectively. The width of the emission peaks is related to the size distribution of GQDs which is in turn related to the synthesis method. The emission wavelength on the other hand is attributed to the functional groups on the edges of GQDs.[17] A distinctive feature between GO-GQDs and CA-GQDs is the dependence of the emission on excitation wavelength as shown in Fig. 6. GO-GQDs show an initial red-shift as the excitation wavelength is changed from 340–360 nm, after which the emission wavelength remains unchanged (Fig. 6A). The excitation dependence can be attributed to wider size distribution of the GO-GQDs which is a consequence of the synthesis route. In

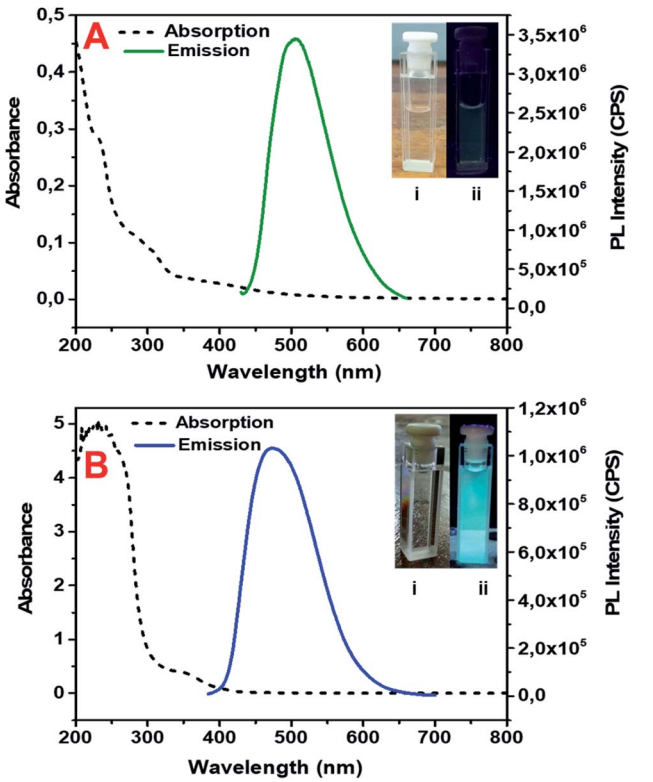

Fig. 5 Absorption and emission spectra of GO-GQDs (A) and CA-GQDs (B). The inset shows the GQDs solution under visible light (i) and under 365 nm UV light (ii).

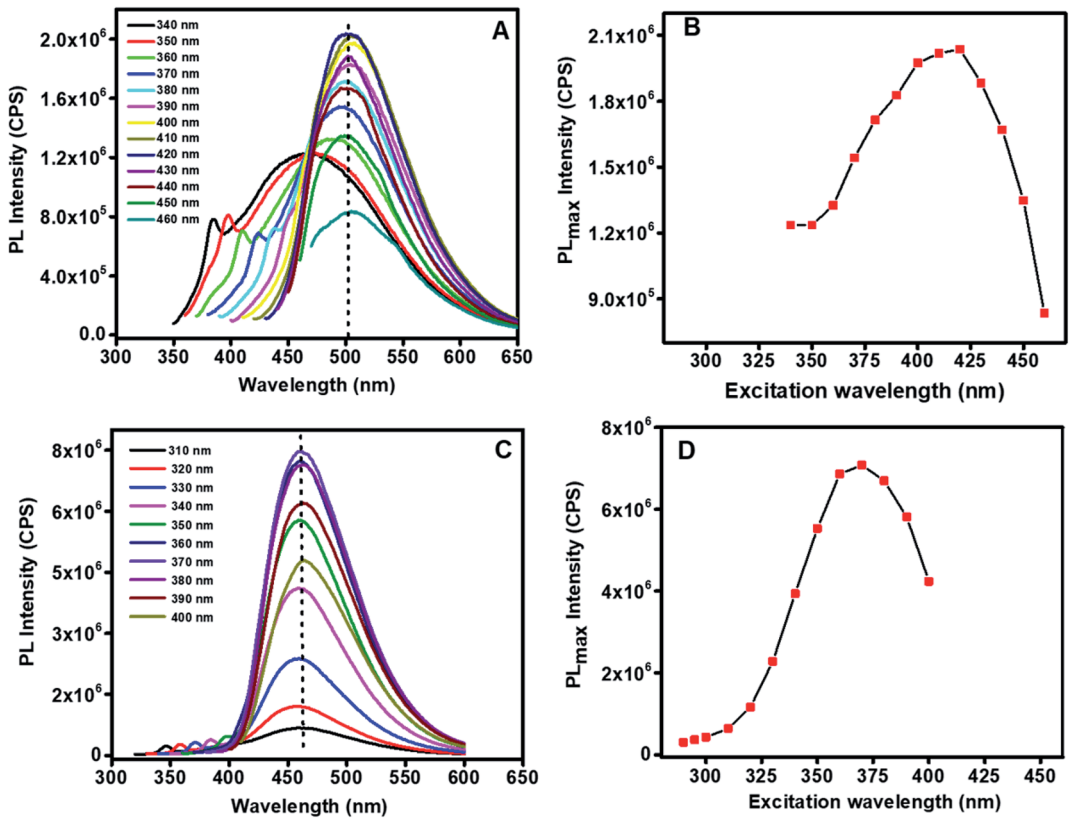

Fig. 6 The effect of excitation wavelength on the emission spectra of (A) GO-GQDs and (C) CA-GQDs. (B) and (D) show the effect of excitation wavelength on the maximum PL intensity (PL_{max}) in each case.

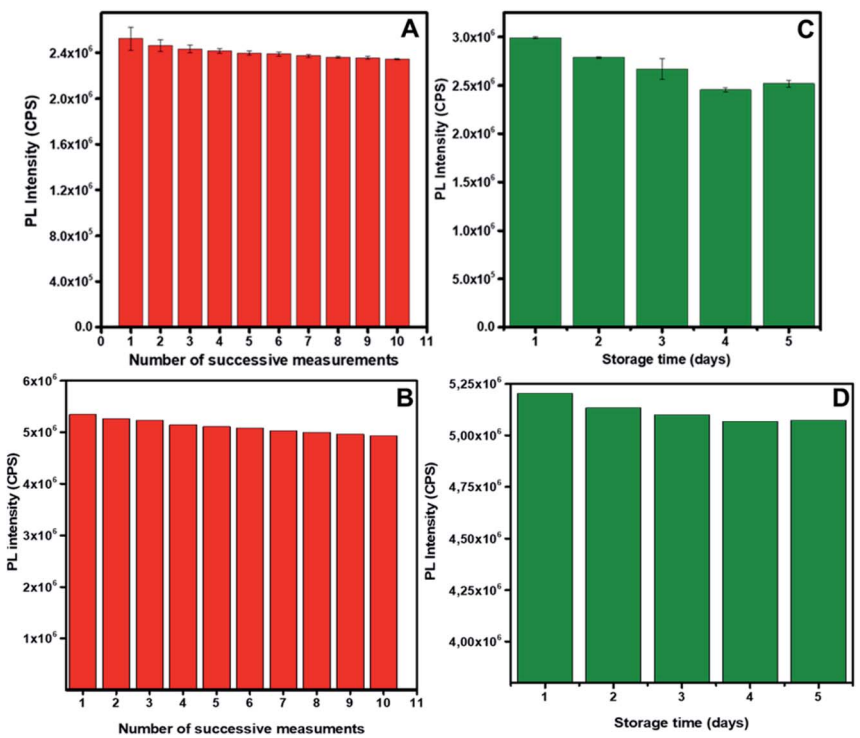

Fig. 7 The effect of successive irradiations at the excitation wavelength for GO-CQDs (A) and CA-GQDs (B). The effect of storage at 4 °C on the stability of the GO-GQDs (B) and CA-GQDs (C).

contrast, CA-GQDs show excitation independent emission (Fig. 6C) which is typical for GQDs made from bottom-up approaches. This can be attributed to uniform size and surface states of the sp^2 clusters present.[31] The fluorescence quantum yields for CA-GQDs and GO-GQDs were found to be 10.2% and 12.2%, respectively.

Both GO-GQDs and CA-GQDs were shown to be photo-stable, as shown in Fig. 7. After ten successive irradiations at the respective excitation wavelengths, the decrease in PL intensity was about 7.1% for GO-GQDs and about 7.6% for CA-GQDs. The effect of storage on the photoluminescence of GQDs is also a critical parameter in their application as sensors. Generally, the photoluminescence of GQDs decreases with storage, and storage at low temperatures has been shown to preserve them. As seen in Fig. 7, storage at 4 °C for both GQDs resulted in minimal decrease in PL intensity (18% for GO-GQDs and 2.3% for CA-GQDs) over a 5 day period, after which they stabilized. This indicates the storage and stabilization period which should at least be allowed before using the GQDs for sensing after synthesis in order to ensure repeatability.

3.5 Fluorescence sensing

The GQDs were applied in detection of the PAH pyrene, as shown in Fig. 9. For both CA-GQDs and GO-GQDs, following the initial treatment with ferric ions as explained in section 2.4, fluorescence enhancement was observed upon addition of increasing concentrations of pyrene. The fluorescence enhancement was linear within the 2–10 $\times$ 10^{-6} mol L^{-1} range. The limit of detection (LOD) and limit of quantitation (LOQ) were determined using the equations $3\delta/K$ and $10\delta/K$, respectively. Where δ is the standard deviation of blank measurements ($n = 10$) and K is the slope of the linear calibration curve. For GO-GQDs the LOD was found to be 0.325 $\times$ 10^{-6} mol L^{-1} and the LOQ was 1.08 $\times$ 10^{-6} mol L^{-1}. For CA-GQDs the LOD was 0.242 $\times$ 10^{-6} mol L^{-1} and the LOQ was 0.807 $\times$ 10^{-6} mol L^{-1}. The CA-GQDs showed better linearity (Fig. 8) and slightly higher sensitivity compared to GO-GQDs which could be attributed to their uniform size distribution as show in the TEM analysis (Fig. 3) which itself is a consequence of the synthesis approach.

3.6 Sensing mechanism

A schematic illustration of the interaction of PAHs and the GQDs treated with Fe is shown in Fig. 9. The fluorescence quenching that was observed upon addition of Fe^{3+} ions could be due to their ability to coordinate with the phenolic hydroxyl groups on the GQD surface, leading to formation of aggregates with neighboring GQDs.[37] The introduction of pyrene weakens these aggregates as it binds with the GQDs through π–π stacking, leading to fluorescence enhancement.

3.7 Application to PAH sensing in real water samples

Water samples obtained from a lake at the University of Pretoria Sports Campus were spiked with different concentrations of pyrene standard solutions within the calibration curve (2–10 $\times$ 10^{-6} mol L^{-1}). The elemental ion composition of the unspiked water sample was also determined using ICP-MS

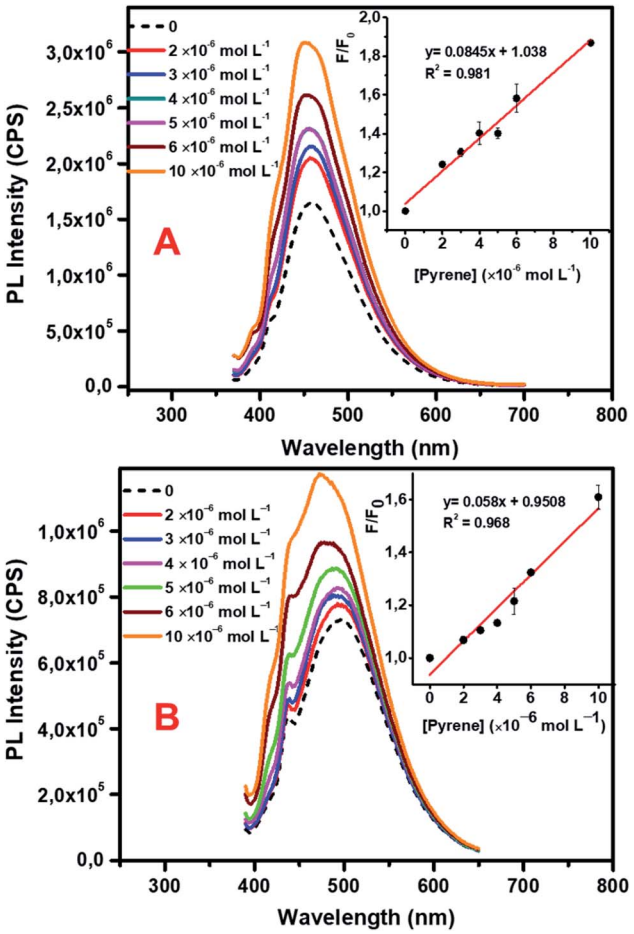

Fig. 8 Fluorescence detection of pyrene using CA-GQDs (A) and GO-GQDs (B). The concentration of pyrene ranged from 2–10 $\times$ 10^{-6} mol L^{-1}. The inset shows a linear response of F/F_0 *versus* concentration where F_0 is the fluorescence intensity of GQDs–Fe^{3+} in the absence of pyrene and F is the fluorescence intensity after interaction with pyrene ($n = 3$).

screening analysis, and the results are shown in Table S1.† Fluorescence detection of the spiked water samples was then carried out following a similar protocol as with standard solutions. The sensor demonstrated satisfactory recoveries ranging from 97–107% (Table 1). This demonstrates that additional metal ions, humic matter, and other matrix components had no effect on the performance of the sensor. Thus, this sensing strategy has excellent potential for application in environmental water samples.

Fluorescence sensing of PAHs by means other graphene based materials has previously been explored[14,15,40,41] and good sensitivity thereof has been reported. However, their application may be limited due to the inclusion of toxic metals, such as in the case of cadmium based QDs as signal transducers. The levels of pyrene in drinking water are reported to range between 14.3 $\times$ 10^{-12}–5.62 $\times$ 10^{-6} mol L^{-1} and between 94.4 $\times$ 10^{-12}–5.87 $\times$ 10^{-6} mol L^{-1} in river water.[7] The proposed sensor developed in this work, despite having a somewhat higher detection limit than other reported methods, uses GQDs of low toxicity for both pre-concentration and signal transduction

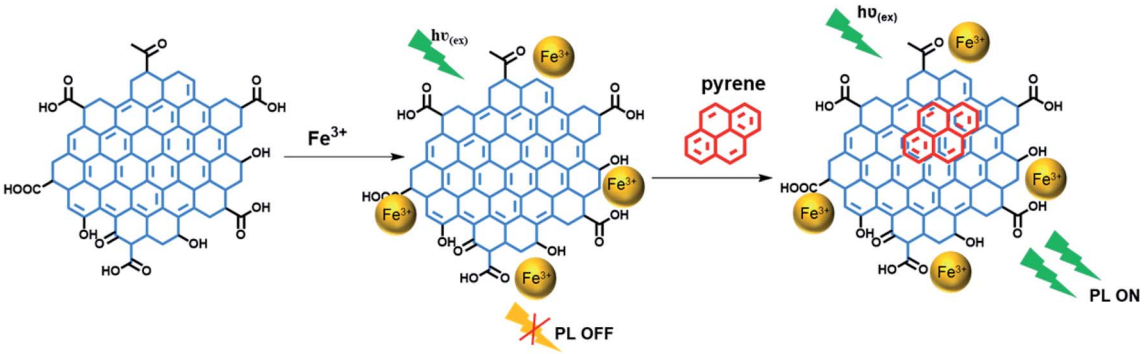

Fig. 9 Schematic illustration of the interaction of GQDs with Fe^{3+} which results in fluorescence quenching. Upon interaction with pyrene the fluorescence is turned on.

Table 1 Recovery tests of pyrene spiked lake water at three different concentrations

Sensing solution	Spiked pyrene concentration ($\times 10^{-6}$ mol L^{-1})	Detected concentration (mean ± SD*, $n = 3$; $\times 10^{-6}$ mol L^{-1})	Recovery (%)
GO-GQDs	4.0	4.1 ± 0.28	102
	6.0	6.2 ± 0.19	103
	10.0	10.0 ± 0.64	107
CA-GQDs	3.0	3.04 ± 0.08	101
	6.0	5.87 ± 0.51	98
	10.0	9.73 ± 0.28	97

(detection) of PAHs. This detection strategy offers promising prospects towards the development of 'green' sensors for environmental PAH monitoring considering that the LODs are within the range of reported concentrations in water.

4. Conclusion

In conclusion, simple synthesis approaches were used to successfully prepare graphene quantum dots, denoted GO-GQDs and CA-GQDs. We further demonstrate the potential application of these GQDs in the detection of pyrene, a common PAH compound in environmental water samples. The interaction of the GQDs with ferric ions led to fluorescence quenching due to aggregation, but subsequent interaction with pyrene through π–π stacking switched on the fluorescence. The detection of pyrene was therefore realized and the detection limits were 0.351×10^{-6} mol L^{-1} and 0.242×10^{-6} mol L^{-1} for GO-GQDs and CA-GQDs, respectively. GQDs have been known to be environmentally friendly, low-cost, and easier to prepare compared to semi-conductor QDs, thus this work paves the way for greener fluorescence monitoring of PAHs. Future work will focus on improving the sensitivity of these sensors and, ultimately to also investigate their reusability and incorporation into portable devices.

Conflicts of interest

We declare are no conflicts of interest.

Acknowledgements

Funding from the University of Pretoria, Water Research Commission (WRC) (Grant K5/2752 and K5/2438), the Photonics Initiative of South Africa (Grant PISA-15DIR-06) and the National Research Foundation of South Africa (post-graduate student bursary (SN) and funding grants 90720 and 93394 (PF)) is gratefully acknowledged. We thank the Microscopy and Microanalysis Laboratory of the University of Pretoria, for their assistance with microscopy measurements.

References

1 L. Van der Wat and P. B. C. Forbes, Lichens as biomonitors for organic air pollutants, *TrAC, Trends Anal. Chem.*, 2015, **64**, 165–172.
2 Z. Zelinkova and T. Wenzl, The occurrence of 16 EPA PAHs in food – a review, *Polycyclic Aromat. Compd.*, 2015, **35**, 248–284.
3 L. Chimuka, P. Sibiya, R. Amdany, E. Cukrowska and P. B. C. Forbes, Status of PAHs in environmental compartments of South Africa: a country report, *Polycyclic Aromat. Compd.*, 2016, **36**, 1–19.
4 H. I. Abdel-Shafy and M. S. M. Mansour, A review on polycyclic aromatic hydrocarbons: source, environmental impact, effect on human health and remediation, *Egypt. J. Pet.*, 2016, **25**, 107–123.
5 P. B. C. Forbes and E. R. Rohwer, Investigations into a novel method for atmospheric polycyclic aromatic hydrocarbon monitoring, *Environ. Pollut.*, 2009, **157**, 2529–2535.

6 V. Bansal, P. Kumar, E. E. Kwon and K.-H. Kim, Review of the quantification techniques for polycyclic aromatic hydrocarbons (PAHs) in food products, *Crit. Rev. Food Sci. Nutr.*, 2015, **51**, 3297–3397.

7 A. Mojiri, J. L. Zhou, A. Ohashi, N. Ozaki and T. Kindaichi, Comprehensive review of polycyclic aromatic hydrocarbons in water sources, their effects and treatments, *Sci. Total Environ.*, 2019, **696**, 133971.

8 ATSDR, *Case studies in environmental medicine toxicity of polycyclic aromatic hydrocarbons (PAHs)*, Agency for Toxic Substances and Disease Registry, 2012.

9 M. Rota, C. Bosetti, S. Boccia, P. Boffetta and C. La Vecchia, Occupational exposures to polycyclic aromatic hydrocarbons and respiratory and urinary tract cancers: an updated systematic review and a meta-analysis to 2014, *Arch. Toxicol.*, 2014, **88**, 1479–1490.

10 A. J. White, P. T. Bradshaw, A. H. Herring, S. L. Teitelbaum, J. Beyea, S. D. Stellman, S. E. Steck, I. Mordukhovich, S. M. Eng, L. S. Engel, K. Conway, M. Hatch, A. I. Neugut, R. M. Santella and M. D. Gammon, Exposure to multiple sources of polycyclic aromatic hydrocarbons and breast cancer incidence, *Environ. Int.*, 2016, **89–90**, 185–192.

11 S. Marzooghi and D. M. Di Toro, A critical review of polycyclic aromatic hydrocarbon phototoxicity models, *Environ. Toxicol. Chem.*, 2017, **36**, 1138–1148.

12 M. Engraff, C. Solere, K. E. C. Smith, P. Mayer and I. Dahllöf, Aquatic toxicity of PAHs and PAH mixtures at saturation to benthic amphipods: linking toxic effects to chemical activity, *Aquat. Toxicol.*, 2011, **102**, 142–149.

13 S. A. Nsibande, H. Montaseri and P. B. C. Forbes, Advances in the application of nanomaterial-based sensors for detection of polycyclic aromatic hydrocarbons in aquatic systems, *TrAC, Trends Anal. Chem.*, 2019, **115**, 52–69.

14 O. Adegoke and P. B. C. Forbes, L-Cysteine-capped core/shell/shell quantum dot–graphene oxide nanocomposite fluorescence probe for polycyclic aromatic hydrocarbon detection, *Talanta*, 2016, **146**, 780–788.

15 O. Adegoke, H. Montaseri, S. A. Nsibande and P. B. Forbes, Alloyed quaternary/binary core/shell quantum dot-graphene oxide nanocomposite: preparation, characterization and application as a fluorescence "switch ON" probe for environmental pollutants, *J. Alloys Compd.*, 2017, **720**, 70–78.

16 L. Li, G. Wu, G. Yang, J. Peng, J. Zhao and J.-J. Zhu, Focusing on luminescent graphene quantum dots: current status and future perspectives, *Nanoscale*, 2013, **5**, 4015–4039.

17 S. Zhu, Y. Song, X. Zhao, J. Shao, J. Zhang and B. Yang, The photoluminescence mechanism in carbon dots (graphene quantum dots, carbon nanodots, and polymer dots): current state and future perspective, *Nano Res.*, 2015, **8**, 355–381.

18 J. Shen, Y. Zhu, X. Yang and C. Li, Graphene quantum dots: emergent nanolights for bioimaging, sensors, catalysis and photovoltaic devices, *Chem. Commun.*, 2012, **48**, 3686–3699.

19 Y. Chong, Y. Ma, H. Shen, X. Tu, X. Zhou, J. Xu, J. Dai, S. Fan and Z. Zhang, The in vitro and in vivo toxicity of graphene quantum dots, *Biomaterials*, 2014, **35**, 5041–5048.

20 S. Wang, I. S. Cole and Q. Li, The toxicity of graphene quantum dots, *RSC Adv.*, 2016, **6**, 89867–89878.

21 X. T. Zheng, A. Ananthanarayanan, K. Q. Luo and P. Chen, Glowing graphene quantum dots and carbon dots: properties, syntheses, and biological applications, *Small*, 2015, **11**, 1620–1636.

22 H. Sun, L. Wu, W. Wei and X. Qu, Recent advances in graphene quantum dots for sensing, *Mater. Today*, 2013, **16**, 433–442.

23 S. Benítez-Martínez and M. Valcárcel, Graphene quantum dots in analytical science, *TrAC, Trends Anal. Chem.*, 2015, **72**, 93–113.

24 L. Lin, M. Rong, F. Luo, D. Chen, Y. Wang and X. Chen, Luminescent graphene quantum dots as new fluorescent materials for environmental and biological applications, *TrAC, Trends Anal. Chem.*, 2014, **54**, 83–102.

25 P. Tian, L. Tang, K. S. Teng and S. P. Lau, Graphene quantum dots from chemistry to applications, *Mater. Today Chem.*, 2018, **10**, 221–258.

26 J. Ju and W. Chen, Graphene quantum dots as fluorescence probes for sensing metal ions: synthesis and applications, *Curr. Org. Chem.*, 2015, **19**, 1150–1162.

27 Q. Liu, K. Wang, J. Huan, G. Zhu, J. Qian, H. Mao and J. Cai, Graphene quantum dots enhanced electrochemiluminescence of cadmium sulfide nanocrystals for ultrasensitive determination of pentachlorophenol, *Analyst*, 2014, **139**, 2912–2918.

28 L. Fan, Y. Hu, X. Wang, L. Zhang, F. Li, D. Han, Z. Li, Q. Zhang, Z. Wang and L. Niu, Fluorescence resonance energy transfer quenching at the surface of graphene quantum dots for ultrasensitive detection of TNT, *Talanta*, 2012, **101**, 192–197.

29 E. Zor, E. Morales-Narváez, A. Zamora-Gálvez, H. Bingol, M. Ersoz and A. Merkoçi, Graphene quantum dots-based photoluminescent sensor: a multifunctional composite for pesticide detection, *ACS Appl. Mater. Interfaces*, 2015, **7**, 20272–20279.

30 G. A. Crosby and J. N. Demas, Measurement of photoluminescence quantum yields. Review, *J. Phys. Chem.*, 1971, **75**, 991–1024.

31 Y. Dong, J. Shao, C. Chen, H. Li, R. Wang, Y. Chi, X. Lin and G. Chen, Blue luminescent graphene quantum dots and graphene oxide prepared by tuning the carbonization degree of citric acid, *Carbon*, 2012, **50**, 4738–4743.

32 W. S. Hummers and R. E. Offeman, Preparation of graphitic oxide, *J. Am. Chem. Soc.*, 1958, **80**, 1339.

33 Y. Zhu, G. Wang, H. Jiang, L. Chen and X. Zhang, One-step ultrasonic synthesis of graphene quantum dots with high quantum yield and their application in sensing alkaline phosphatase, *Chem. Commun.*, 2015, **51**, 948–951.

34 T. V. Tam, N. B. Trung, H. R. Kim, J. S. Chung and W. M. Choi, One-pot synthesis of N-doped graphene quantum dots as a fluorescent sensing platform for Fe^{3+} ions detection, *Sens. Actuators, B*, 2014, **202**, 568–573.

35 A. Ananthanarayanan, X. Wang, P. Routh, B. Sana, S. Lim, D.-H. Kim, K.-H. Lim, J. Li and P. Chen, Facile synthesis of graphene quantum dots from 3D graphene and their

application for Fe^{3+} sensing, *Adv. Funct. Mater.*, 2014, **24**, 3021–3026.

36 Y.-L. Zhang, L. Wang, H.-C. Zhang, Y. Liu, H.-Y. Wang, Z.-H. Kang and S.-T. Lee, Graphitic carbon quantum dots as a fluorescent sensing platform for highly efficient detection of Fe^{3+} ions, *RSC Adv.*, 2013, **3**, 3733–3738.

37 X. Zhu, Z. Zhang, Z. Xue, C. Huang, Y. Shan, C. Liu, X. Qin, W. Yang, X. Chen and T. Wang, Understanding the selective detection of Fe^{3+} based on graphene quantum dots as fluorescent probes: The Ksp of a metal hydroxide-assisted mechanism, *Anal. Chem.*, 2017, **89**, 12054–12058.

38 R. Álvarez-Diduk, J. Orozco and A. Merkoçi, Paper strip-embedded graphene quantum dots: a screening device with a smartphone readout, *Sci. Rep.*, 2017, **7**, 976.

39 Y. Wang, S. Kalytchuk, Y. Zhang, H. Shi, S. V. Kershaw and A. L. Rogach, Thickness-dependent full-color emission tunability in a flexible carbon dot lonogel, *J. Phys. Chem. Lett.*, 2014, **5**, 1412–1420.

40 L. Wang, Z. Huang, Q. Gao, Y. Liu, X. Kou and D. Xiao, A novel pyrene fluorescent sensor based on the π–π Interaction between pyrene and graphene of graphene–cadmium telluride quantum dot nanocomposites, *Spectrosc. Lett.*, 2015, **48**, 748–756.

41 C. Carrillo-Carrión, B. M. Simonet and M. Valcárcel, Carbon nanotube–quantum dot nanocomposites as new fluorescence nanoparticles for the determination of trace levels of PAHs in water, *Anal. Chim. Acta*, 2009, **652**, 278–284.

